Astronomy & Astrophysics manuscript no. 40868corr
April 16, 2021

Upper limits for phosphine (PH_3) in the atmosphere of Mars

K. S. Olsen[1], A. Trokhimovskiy[2], A. S. Braude[3], O. I. Korablev[2], A. A. Fedorova[2], C. F. Wilson[1], M. R. Patel[4], P. G. J. Irwin[1], F. Montmessin[3], F. Lefèvre[3], L. Baggio[3], J. Alday[1], D. A. Belyaev[2], A. Patrakeev[2], and A. Shakun[2]

[1] Department of Physics, University of Oxford, Oxford, UK
e-mail: Kevin.Olsen@physics.ox.ac.uk
[2] Space Research Institute (IKI), Moscow, Russia
[3] Laboratoire Atmosphères, Milieux, Observations Spatiales (LATMOS/CNRS), Paris, France
[4] School of Physical Sciences, The Open University, Milton Keynes, UK

Received January X, 2021

ABSTRACT

Phosphine (PH_3) is proposed to be a possible biomarker in planetary atmospheres and has been claimed to have been observed in the atmosphere of Venus, sparking interest in the habitability of Venus's atmosphere. Observations of another biomarker, methane (CH_4), have been reported several times in the atmosphere of Mars, hinting at the possibility of a past or present biosphere. The Atmospheric Chemistry Suite on the ExoMars Trace Gas Orbiter has a spectral range that includes several absorption lines of PH_3 with line strengths comparable to previously observed CH_4 lines. The signature of PH_3 was not observed in the 192 observations made over a full Martian year of observations, and here we report upper limits of 0.1–0.6 ppbv.

1. Introduction

Phosphate (PO_4^{3-}) is an essential molecule for all forms of life on Earth. Phosphine (PH_3) is a very reactive, rapidly photolyzed, and highly variable component of the terrestrial atmosphere. Found at parts per trillion by volume (pptv) to parts per billion (ppbv) volume mixing ratios (VMRs), it accounts for approximately 10% of Earth's atmospheric phosphorus (Glindemann et al. 2003; Elm et al. 2017). It does not play a direct role in Earth's biology but acts as an exchange path for phosphorous, being emitted from the biosphere, oxidized to phosphoric acid (H_3PO_4), and then taken up again in biological systems. The dominant sources of phosphine in the terrestrial atmosphere are emissions from soils, sediments, and manures (Glindemann et al. 2005a). In contrast, abiotic PH_3 production may be ongoing in the hot and reducing deep atmospheres of Saturn and Jupiter (e.g. Bregman et al. 1975; Burgdorf et al. 2004; Fletcher et al. 2009).

Phosphine may play a role in the anaerobic biological systems of anoxic environments, where it will not be readily oxidized (Bains et al. 2019; Sousa-Silva et al. 2020). One such proposed environment is the cloud decks of Venus (Seager et al. 2020). Thus, when the first detection of a phosphine absorption line (at 1.123 mm) in the Venusian atmosphere was announced (Greaves et al. 2020c), it was hailed as evidence of a possible microbial habitat in the upper atmosphere of Venus. The result has since been criticized on technical grounds (Snellen et al. 2020; Villanueva et al. 2020; Thompson 2021; Akins et al. 2021; Lincowski et al. 2021), and other observations did not corroborate it (Encrenaz et al. 2020; Trompet et al. 2021); however, the original team stands by their findings (Greaves et al. 2020b,a) and has reported revised mixing ratios of 5–20 ppbv.

On Mars, methane is another possible biomarker that has been tentatively detected (Formisano et al. 2004; Krasnopolsky et al. 2004; Mumma et al. 2009; Webster et al. 2015; Giuranna et al. 2019), though not confirmed by the ExoMars Trace Gas Orbiter (TGO; Korablev et al. 2019), and thus measurements of phosphine may be able to help identify its source. For example, identifying methane and phosphine would hint towards a biological source of methane, whereas finding methane alongside sulphur species would imply a geologic source of both trace gases.

The primary objective of the ExoMars TGO mission is to search for undetected trace gases diagnostic of active geological or biogenic processes (Vago et al. 2015). To this end, it carries two spectrometer suites, the Atmospheric Chemistry Suite (ACS; Korablev et al. 2018) and the Nadir and Occultation for Mars Discovery (NOMAD; Vandaele et al. 2018), which both offer unprecedented sensitivity due to their fine spectral resolutions and solar occultation technique. Phosphine (PH_3) was not an initial target gas of ExoMars and was not proposed as a possible biomarker prior to the arrival of the TGO in Martian orbit in 2018 (Seager et al. 2016; Schwieterman et al. 2018). However, some of the strongest infrared absorption lines that do not overlap with the CO_2 ν_3 absorption band lie within the spectral range of the ACS mid-infrared channel (ACS MIR), providing an opportunity to search for the signature of PH_3 in the atmosphere of Mars.

So far, neither the biomarker CH_4 nor the related gases C_2H_4 and C_2H_6 have been observed with ACS or NOMAD (Korablev et al. 2019; Knutsen et al. 2021; Montmessin et al. 2021). Here, we report new upper limits for phosphine in the atmosphere of Mars of 0.2 ppbv above 10 km.

2. Observations

ACS is a suite of three spectrometers: The thermal infrared channel (TIRVIM) is a compact Fourier transform spectrometer with a spectral range of 1.7 to 17 μm; the near-infrared channel (NIR) combines an echelle grating with an acousto-optical tunable filter and covers the range 1 to 1.7 μm; and ACS MIR is a cross-dispersion spectrometer consisting of an echelle grating and a secondary, steerable reflecting diffraction grating. ACS MIR has the finest spectral resolution of any remote sensing mission to

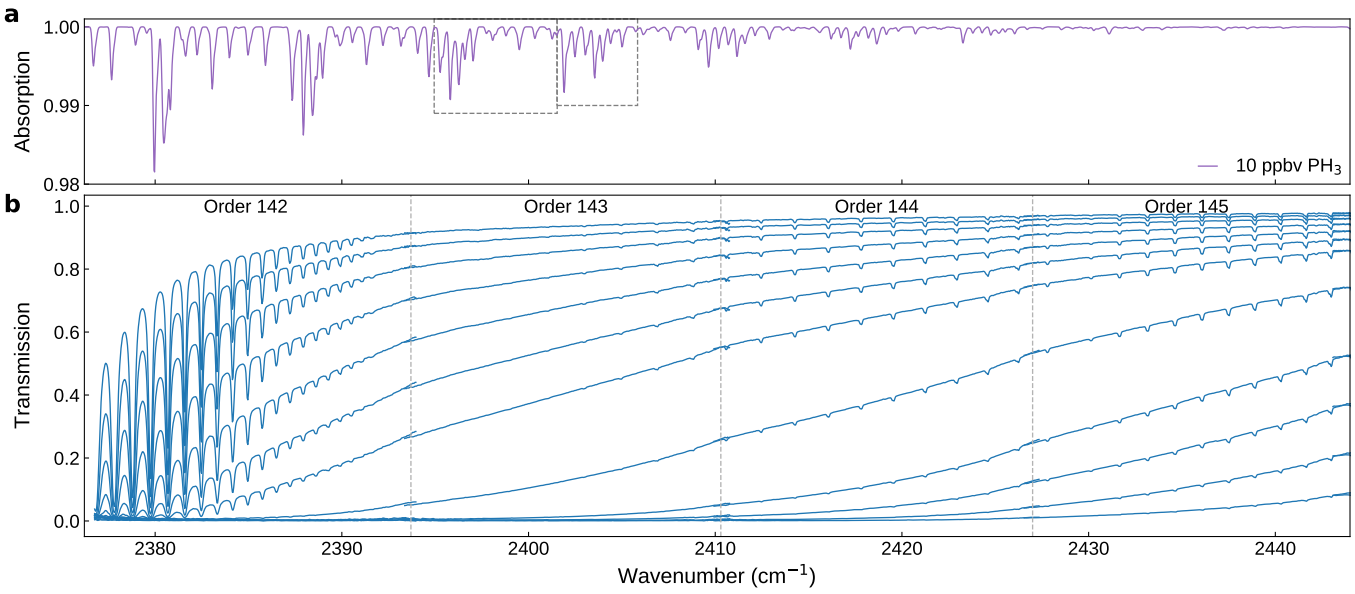

Fig. 1. Spectral range of ACS MIR containing PH_3 absorption features. *Panel a*: Modelled transmission spectrum contributions from 10 ppbv of PH_3 from a 20 km tangent height. *Panel b*: Single spectra extracted from orders 142–145 for 12 consecutive tangent heights (2–26 km) in the lower atmosphere of Mars using ACS MIR secondary grating position 9. All visible absorption lines result from CO_2, which also impacts the broad continuum that decreases transmission towards lower wavenumbers, where the CO_2 ν_3 vibration-rotation band is centred. Boxes in panel *a* indicate the spectral windows covering PH_3 absorption features in order 143 used to determine upper limits.

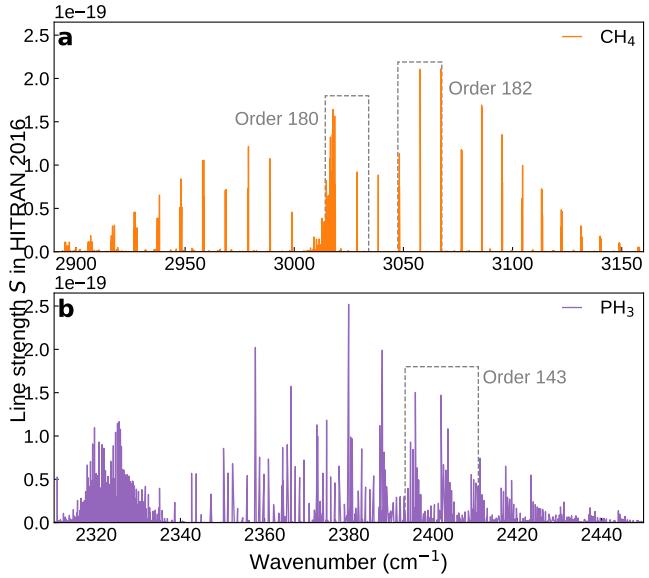

Fig. 2. HITRAN 2016 line strengths for the ν_3 vibration-rotation band of CH_4 (*panel a*) and the ν_3 vibration-rotation band of PH_3 (*panel b*). The spectral ranges of important ACS MIR diffraction orders are indicated in grey.

Mars to date ($\lambda/\Delta\lambda \sim 30,000$) and covers a spectral range of 2400 to 4400 cm^{-1} (2.2 to 4.2 μm; Korablev et al. 2018).

ACS MIR operates in solar occultation mode, recording a series of spectra with tangent height spacings of 1–2 km by using the Sun as a light source and observing the limb of the atmosphere. The secondary diffraction grating separates diffraction orders that would otherwise overlap in the infrared spectral region. Observations are measured with a two-dimensional detector array. The horizontal axis corresponds to the wavenumber, and the vertical axis corresponds firstly to the diffraction order and secondly to the vertical field of view of the instrument. Each order appears as a stripe across the detector, the width of which covers around 20 rows of pixels, each row producing a unique spectrum recorded ~ 0.2 km above or below the adjacent rows. Thus, at every tangent height several spectra are recorded for each order, representing a vertical range of several kilometres. Details about the instrument and data processing, as well as example detector image frames, can be found in Korablev et al. (2018), Korablev et al. (2019), Trokhimovskiy et al. (2020), and Olsen et al. (2021a).

The absorption signature for PH_3 can be sought by using secondary grating position 9, which provides access to diffraction orders 142–152, covering the spectral range 2377–2560 cm^{-1}; these are the lowest wavenumbers available to ACS MIR. Figure 1a shows modelled PH_3 absorption features with ACS MIR spectral resolution, indicating the locations of the most significant PH_3 absorption features over orders 142–143. Figure 1b shows example spectra from the same orders recorded during one occultation. At each tangent height, a single spectrum was extracted for each order. The change in baseline transmittance is mainly due to increasing aerosol extinction as tangent heights approach the surface. The left side of the spectrum is dominated by the strong ν_3 vibration-rotation band of CO_2, the continuum absorption of which also impacts the transmittance of adjacent orders. While the strongest PH_3 lines directly overlap the CO_2 ν_3 band, prominent lines free of interference remain in order 143, which is where this study focuses (lines in order 144 are too weak, and interference from CO_2 is too strong in order 142; see Fig. 1).

The line strengths of the strongest PH_3 lines in this spectral region are about 1.5×10^{-19} in the 2016 edition of the HITRAN database, which is used in the forward modelling in this study (Gordon et al. 2017, we note that Greaves et al. 2020c used the ExoMol line list for high temperatures). This is comparable to those used by ACS MIR and others to search for methane. Figure 2 shows the line strengths of the ν_3 band of methane and

the ν_3 band of phosphine, with the spectral ranges of diffraction orders used to search for them indicated. The expectation, then, is that ACS MIR should have roughly similar sensitivity to both trace gases, of the order of less than a part per billion. Upper limits for methane from the ACS MIR data are lower than for PH_3, around tens to hundreds of pptv (Korablev et al. 2019).

The ExoMars TGO entered Mars orbit in late 2016, and its nominal science phase commenced in April 2018. It is approaching 1.5 Mars years (MYs) of coverage (three Earth years). The dataset analysed here consists of all 192 usable occultations recorded between L_s = 140–350° in both MY 34 and 35 (we note that there was a period between MYs in which position 9 was not used). The majority of observations are at high northern or southern latitudes (around 60°N and -60°S), but several low latitude observations were also made.

3. Results

To make the most accurate measurements of rare trace gases possible, we exploited the vertical field of view of the ACS MIR instrument and considered 12 spectra for diffraction order 143 from each detector frame recorded at each observation in the occultation series. Each spectrum has a unique tangent altitude, with corresponding temperatures and pressures, and some also have a unique instrument line shape (ILS) that needed to be fitted prior to VMR retrievals. The ILS was impacted by an optical aberration that caused the total absorption to be divided into a primary and secondary image (Alday et al. 2019; Olsen et al. 2021a) that had to be accounted for. The accuracy of retrievals using a fitted ILS for ACS MIR was verified by comparing retrieved vertical profiles of temperature, pressure, water vapour, and carbon monoxide with simultaneous observations made with ACS NIR (Alday et al. 2019; Fedorova et al. 2020; Olsen et al. 2021a).

To best account for the observational differences affecting adjacent spectra, each of the 12 detector rows from which spectra were extracted was treated as a unique solar occultation sequence and analysed independently. The upper limits were derived from the mean of the 12 retrieved VMR vertical profiles. This method was developed to examine the weak signature of HDO in the upper atmosphere towards the hygropause but has effectively been used to study hydrogen chloride (HCl) Olsen et al. (2021b), the first novel trace gas discovered by ACS MIR (Korablev et al. 2021). Vertical profiles of temperature and pressure are independently measured by simultaneous observations with ACS NIR, which observes a CO_2 band at 1.38 μm (7250 cm^{-1}). Spectral fitting is done with the Jet Propulsion Laboratory's Gas Fitting software suite (GFIT or GGG) (Sen et al. 1996; Irion et al. 2002; Wunch et al. 2011).

Vertical profiles of a fitted gas's VMR were retrieved by inverting the matrices of line-of-sight optical paths through the atmospheric layers with the matrices of estimated number densities derived from the spectral fits at each altitude. Two fitting windows covering the strongest features in order 143 were used (2394.95–2401.53 cm^{-1} and 2401.52–2405.84 cm^{-1}; see Fig. 1). Uncertainties were computed from the Jacobian matrix of partial derivatives. Additional details about spectral fitting and VMR retrievals can be found in Olsen et al. (2020), Olsen et al. (2021a), and Korablev et al. (2021), and details about the analysis method used here can be found in Olsen et al. (2021b).

Figure 3a shows an example of the ACS MIR data and helps to illustrate the PH_3 analysis technique. For one occultation, at a tangent height near 13 km, each row extracted from order 143 in the detector frame has been normalized and is shown. Also shown is the mean spectrum, with greatly reduced instrument noise (the root mean square of fitting residuals is reduced from $\sim$ 0.0014 to 0.0008). The observed absorption lines are due to CO_2, and two best-fit lines are shown, for which PH_3 abundances were fixed in order to illustrate where PH_3 features would be found. We note that the noise to the left, near 2396 cm^{-1}, is larger than elsewhere. This is because it is near the edge of the detector frame and has a lower signal strength. We also note that there appears to be a systematic error fitting the CO_2 lines from left to right; this is due to the normalization of the spectra, which can safely remove the impact of aerosols under normal circumstances but should not be performed in this region due to the CO_2 continuum near the CO_2 ν_3 band. Normalization was not used when computing detection limits; it is only used in Fig. 3a to facilitate the comparison of the spectra and to illustrate the line locations of PH_3 absorption features, the impact that 10 ppbv of PH_3 would have, and the noise level of ACS MIR spectra.

To determine whether PH_3 was detected, we considered the set of 12 retrieved VMR vertical profiles. We computed the weighted mean, using the uncertainty (σ) of each retrieval as weights ($1/\sigma^2$), and computed the standard error of the weighted mean. Figure 3b shows the VMR vertical profile retrieval uncertainties for the 12 sets of solar occultation spectra from which those shown in Fig. 3a were taken. Also shown are the retrieval uncertainties derived using the mean spectra, which are lower than those of the individual spectra due to the reduced noise, but still greater than the standard error of the weighted mean, which is the uncertainty of the mean retrieved VMR vertical profile.

If the retrieved VMR was greater than three or five times the standard error, we considered it to be a possible detection. We would then verify it by examining the ensemble of spectra and mean spectra at each altitude. However, no candidate detections were found.

In the absence of any detection, we interpreted the vertical profile of the standard error of the weighted mean as an upper limit to the detection. These 1σ upper limits are shown in Fig. 4 for the entire ACS MIR dataset recorded thus far using secondary grating position 9. Each profile is coloured by the density of observations, derived using a Gaussian kernel density estimation for the entire dataset. The density is low below 10 km due to differences in the lowest observable tangent height. That is, only a fraction of the occultations are clearly able to probe the lowest layers of the atmosphere due to aerosol extinction (dust is present during most of the observation period). Above 50 km, the differences are related to the total number density, which varies with the latitude and time of observation.

4. Discussion and conclusions

The highest density of derived upper limits occurs near 30 km and at a detection limit of $\sim$ 0.6 ppbv. The lowest values are $<$ 0.2 ppbv and are reached at altitudes between 10 and 35 km. These are comparable to the reported upper limits in Korablev et al. (2019) for CH_4 of 0.15 ppbv. While several ACS MIR observations led to CH_4 detection limits of the order of tens of pptv, we must note that the *R*-branch CH_4 lines available are stronger than the PH_3 lines in Fig. 3 (e.g. compare to Fig. 2), and they are more towards the centre of their diffraction orders, which leads to a higher signal-to-noise ratio. Furthermore, potential CH_4 lines are not subject to the strong absorption of the CO_2 ν_3 continuum, which effectively reduces the line depth relative to the noise. We also note that, relative to the Venusian observations of 20 ppbv, the line strengths of PH_3 in the ACS MIR spectral range ($\sim$ 1.5×10^{-19}) are much larger than that

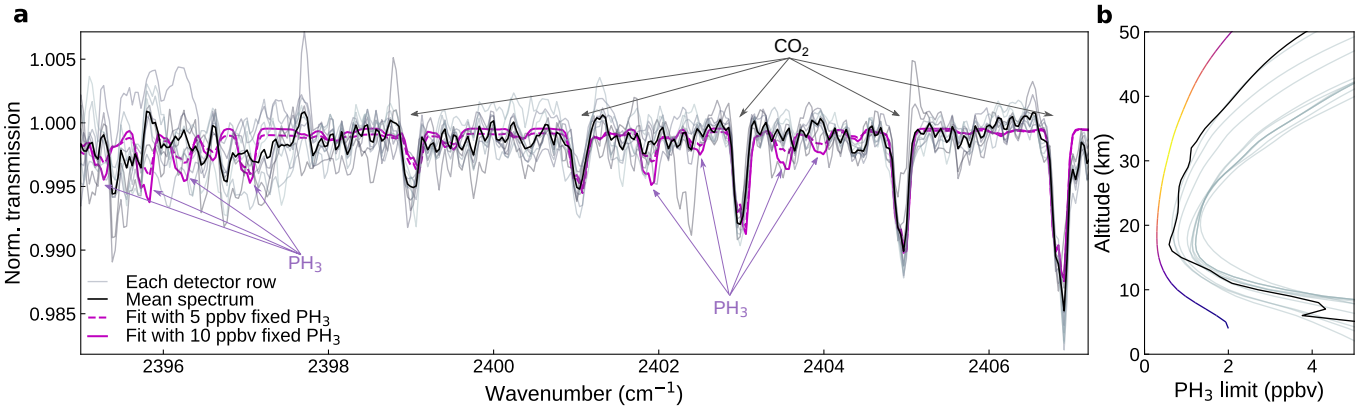

Fig. 3. Example ACS MIR spectra and upper limits for PH_3. *Panel a*: Normalized spectra for diffraction order 143 extracted from a single detector frame observed near 13 km tangent height. The lines in various shades of grey are the individual normalized spectra, the black line is a mean spectrum, and the dashed and solid purple lines are best-fit lines to the mean spectrum with two fixed quantities of PH_3, 5 and 10 ppbv, respectively. *Panel b*: 1σ detection limits derived from non-normalized spectra (shades of grey) and from the mean spectrum (black). The standard error computed from all 12 sets of spectra is also shown, as in Fig. 4. The detection limit derived near 13 km is 0.5 ppbv for the entire occultation and 1.5-2.5 ppbv for the individual extracted detector rows.

of the single line claimed in Venus's atmosphere (1.27×10^{-22}) Greaves et al. (2020c).

Had PH_3 been detected at Mars, a biological origin would not be certain. The Martian environment is not anoxic, unlike the environments proposed by Sousa-Silva et al. (2020), and biogenic (or other) PH_3 may be removed by rapid oxidation by the hydroxyl radical (OH), itself a by-product of water vapour photolysis.

While ACS MIR observations have not detected any sulphur species indicative of a geological source of methane, they have detected hydrogen chloride, which may have a magmatic or volcanic source (Korablev et al. 2021). However, ACS MIR has also not detected any signatures of methane in the atmosphere of Mars (Montmessin et al. 2021). Phosphorous is found on the surface of Mars (e.g. Gellert et al. 2004; Rieder et al. 2004), and phosphate has been identified in Martian meteorites (e.g. McCubbin & Nekvasil 2008; Agee et al. 2013). Though not favoured, there are abiotic processes that may release PH_3 gas from the surface (Glindemann et al. 2004, 2005b), and volcanic processes have even been proposed to explain its presence on Venus (Truong & Lunine 2020).

Thus, while PH_3 has been proposed as a possible biomarker for anoxic exoplanetary environments, it is not observed in the atmosphere of Mars, where the biomarker CH_4 had previously been reported (although we note that these reports remain controversial and have not been corroborated by the ExoMars TGO). Due to the highly oxidative state of the Martian atmosphere, however, its presence was perhaps unexpected. An upper limit of 0.2–0.6 ppbv is set for the atmosphere of Mars between 10 and 45 km.

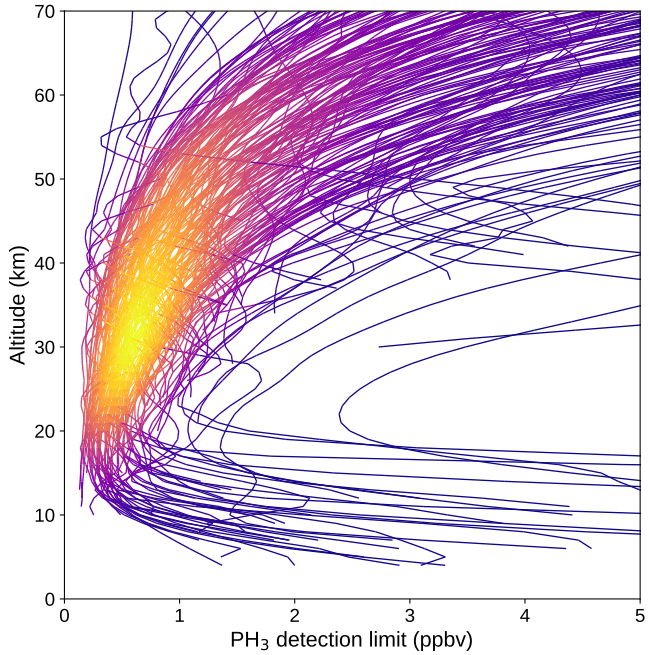

Fig. 4. Vertical profiles of the standard error of the weighted mean for 192 ACS MIR solar occultations observed between L_s = 140–350° in MY 34 and 35. The lines are coloured by the Gaussian kernel density estimate for the entire dataset, with the highest density of data appearing as orange and yellow.

Acknowledgements. The ACS investigation was developed by the Space Research Institute (IKI) in Moscow, and the Laboratoire Atmosphères, Milieux, Observations Spatiales (LATMOS/CNRS) in Paris. The investigation was funded by Roscosmos, the National Centre for Space Studies of France (CNES) and the Ministry of Science and Education of Russia. The GGG software suite is maintained at JPL (tccon-wiki.caltech.edu). This work was funded by the UK Space Agency (ST/T002069/1, ST/V002295/1). All spectral fitting was performed by KSO using the GGG software suite. The interpretation of the results was done by KSO, AT, ASB, PGJI, MP, OK, FM, and FL. The processing of ACS spectra is done at IKI by AT and at LATMOS by LB. Input and aid on spectral fitting were given by JA, DAB, AF, and CFM. The ACS instrument was designed, developed, and operated by AP, AS, AT, FM, and OK. Vertical profiles of measured temperature and pressure were generated by AF.

References

Agee, C. B., Wilson, N. V., McCubbin, F. M., et al. 2013, Science, 339, 780
Akins, A. B., Lincowski, A. P., Meadows, V. S., & Steffes, P. G. 2021, Astrophys. J. Lett., 907, L27
Alday, J., Wilson, C. F., Irwin, P. G. J., et al. 2019, Astron. Astrophys., 630, A91
Bains, W., Jurand Petkowski, J., Sousa-Silva, C., & Seager, S. 2019, Astrobiology, 19, 885
Bregman, J. D., Lester, D. F., & Rank, D. M. 1975, Astrophys. J., 202, L55
Burgdorf, M. J., Orton, G. S., Encrenaz, T., et al. 2004, Adv. Space Res., 34, 2247
Elm, J., Myllys, N., & Kurtén, T. 2017, Mol. Phys., 115, 2168

Encrenaz, T., Greathouse, T. K., Marcq, E., et al. 2020, Astron. Astrophys., 643, L5
Fedorova, A. A., Montmessin, F., Korablev, O., et al. 2020, Science, 367, 297
Fletcher, L. N., Orton, G. S., Teanby, N. A., & Irwin, P. G. J. 2009, Icarus, 202, 543
Formisano, V., Atreya, S., Encrenaz, T., Ignatiev, N., & Giuranna, M. 2004, Science, 306, 1758
Gellert, R., Rieder, R., Anderson, R. C., et al. 2004, Science, 305, 829
Giuranna, M., Viscardy, S., Daerden, F., et al. 2019, Nat. Geosci., 1752
Glindemann, D., Edwards, M., & Kuschk, P. 2003, Atmosph. Environ., 37, 2429
Glindemann, D., Edwards, M., Liu, J., & Kuschk, P. 2005a, Ecol. Eng., 24, 457
Glindemann, D., Edwards, M., & Morgenstern, P. 2005b, Environ. Sci. Technol., 39, 8295
Glindemann, D., Edwards, M., & Schrems, O. 2004, Atmos. Environ., 38, 6867
Gordon, I. E., Rothman, L. S., Hill, C., et al. 2017, J. Quant. Spectrosc. Radiat. Transfer, 203, 3
Greaves, J. S., Bains, W., Petkowski, J. J., et al. 2020a, arXiv e-prints, arXiv:2012.05844
Greaves, J. S., Richards, A. M. S., Bains, W., et al. 2020b, arXiv e-prints, arXiv:2011.08176
Greaves, J. S., Richards, A. M. S., Bains, W., et al. 2020c, Nat. Astron.
Irion, F. W., Gunson, M. R., Toon, G. C., et al. 2002, Appl. Opt., 41, 6968
Knutsen, E. W., Villanueva, G. L. Liuzzi, G., Crismani, M. M. J., et al. 2021, Icarus
Korablev, O., Montmessin, F., Trokhimovskiy, A., et al. 2018, Space Sci. Rev., 214, 7
Korablev, O., Olsen, K. S., Trokhimovskiy, A. andLefèvre, F., et al. 2021, Sci. Adv., 7, eabe4386
Korablev, O., Vandaele, A. C., Montmessin, F., et al. 2019, Nature, 568, 517
Krasnopolsky, V. A., Maillard, J. P., & Owen, T. C. 2004, Icarus, 172, 537
Lincowski, A. P., Meadows, V. S., Crisp, D., et al. 2021, Astrophys. J. Lett., 908, L44
McCubbin, F. M. & Nekvasil, H. 2008, Am. Min., 93, 676
Montmessin, F., Korablev, O. I., Trokhimovskiy, A., et al. 2021, Astron. Astrophys.
Mumma, M. J., Villanueva, G. L., Novak, R. E., et al. 2009, Science, 323, 1041
Olsen, K. S., Lefèvre, F., Montmessin, F., et al. 2021a, Nat. Geosci., 14, 67
Olsen, K. S., Lefèvre, F., Montmessin, F., et al. 2020, Astron. Astrophys., 639, A141
Olsen, K. S., Trokhimovskiy, A., Montabone, L., et al. 2021b, Astron. Astrophys.
Rieder, R., Gellert, R., Anderson, R. C., et al. 2004, Science, 306, 1746
Schwieterman, E. W., Kiang, N. Y., Parenteau, M. N., et al. 2018, Astrobiology, 18, 663
Seager, S., Bains, W., & Petkowski, J. J. 2016, Astrobiology, 16, 465
Seager, S., Petkowski, J. J., Gao, P., et al. 2020, Astrobiology, 21
Sen, B., Toon, G. C., Blavier, J.-F., Fleming, E. L., & Jackman, C. H. 1996, J. Geophys. Res., 101, 9045
Snellen, I. A. G., Guzman-Ramirez, L., Hogerheijde, M. R., Hygate, A. P. S., & van der Tak, F. F. S. 2020, Astron. Astrophys., 644, L2
Sousa-Silva, C., Seager, S., Ranjan, S., et al. 2020, Astrobiology, 20, 235
Thompson, M. A. 2021, Mon. Not. Roy. Astron. Soc., 501, L18
Trokhimovskiy, A., Perevalov, V., Korablev, O., et al. 2020, Astron. Astrophys., 639, A142
Trompet, L., Robert, S., Mahieux, A., et al. 2021, Astron. Astrophys., 645, L4
Truong, N. & Lunine, J. I. 2020, arXiv e-prints, arXiv:2009.11904
Vago, J., Witasse, O., Svedhem, H., et al. 2015, Sol. Syst. Res., 49, 518
Vandaele, A. C., Lopez-Moreno, J.-J., Patel, M. R., et al. 2018, Space Sci. Rev., 214, 80
Villanueva, G., Cordiner, M., Irwin, P., et al. 2020, arXiv e-prints, arXiv:2010.14305
Webster, C. R., Mahaffy, P. R., Atreya, S. K., et al. 2015, Science, 347, 415
Wunch, D., Toon, G. C., Blavier, J. L., et al. 2011, Phil. Trans. R. Soc. A, 369, 2087